

Supplementary material for ‘Quantitative reconstruction of pore pressure history in sedimentary basins using fluid escape pipes’

Joe Cartwright¹, Chris Kirkham¹, Martino Foschi¹, Neil Hodgson², Karyna Rodriguez² and David James³

¹ Department of Earth Sciences, University of Oxford, South Parks Road, Oxford, OX1 3 AN, UK

² Searcher, Unit 6, Albion House, High Street, Woking, GU21 6BG

³ Cwmystwyth, Ceredigion, Wales

SEISMIC AND WELL DATA

A 3D seismic survey acquired and processed by Spectrum (now TGS) was used for the study, along with selected profiles from two regional 2D seismic surveys. The data was interpreted and all key horizons were mapped using Petrel software. Further details can be found in Cartwright et al. (2018) and Kirkham et al. (2019).

TIMING OF FOLD PHASES

The growth history of the Oceanus pre-salt anticline involves two main phases of tectonic compression linked to regional plate boundary changes. The first is evidenced by the syn-kinematic packages of the Mid to Late Miocene units thinning onto the fold crests. The second phase occurred during the Pliocene to Recent, and is evidenced by the substantial structural relief

at the base of the salt sheet (Fig. 2; Fig. S3). Regional tectonic reconstructions of the Dead Sea Transform have suggested a renewed phase of activity from 3 Ma in the adjacent regions of Lebanon (Gomez et al. 2007), and the Latakia Ridge (Hall et al. 2005) which points to rejuvenated growth of offshore pre-salt anticlines occurring at approximately the same time. Continued growth of these folds during the critical period of the last 2 million years is thus consistent with the regional tectonic context, and would require a state of stress to be characterised by a horizontal and NW-SE oriented maximum compressive stress.

FORMATION OF FLUID ESCAPE PIPES BY NATURAL HYDRAULIC FRACTURING

A number of mechanisms have been suggested to explain the formation of fluid escape pipes, including hydraulic fracturing, solution collapse, and fluidisation (see review in Cartwright and Santamarina, 2015). For fluid escape pipes that transect thick salt sequences however, it has recently been argued that hydraulic fracturing offers the only plausible mechanism (Kirkham et al. 2018). This argument is based on the co-occurrence of fluid escape pipes with pockmarks and small mounded extrusive bodies (mud volcanoes) at their outlets in a region of the West Nile Delta, and where both sets of conduits transected a thick salt sequence en route from the source region to the contemporaneous seabed. Fluidisation is not viable in an evaporite layer, and solution collapse would only occur locally before brine saturations exceed the halite solubility threshold. Hydraulic fracture networks offer the only viable explanation for the fluxes implied by the extrusion of the mud volcanoes.

The fluid escape pipes in the study area are identical in their dimensions and seismic character to those described by Kirkham et al. (2018), and by analogy therefore, we assume that a similar formation mechanism applied. The detailed geometry of the postulated hydraulic fracture networks

are unknown, however, so we simply assume that fluid pressures must have been sufficient to initiate and propagate small scale (10s of metres) hydraulic fractures in the generalised zone imaged by the seismic pipe structure (see Cartwright and Santamarina, 2015). This assumption underpins our use of the local fracture gradient in the sealing intervals above the reservoir to compute the minimum pressure required for pipe formation. This conservative view does not take into account possible complicating factors relating to multiphase flow, gas exsolution, or wall rock collapse. Similarly, we are not able to compute the dynamic pressure gradient of the fluid flowing upwards in the pipe.

METHODOLOGY FOR CONSTRUCTING THE PRESSURE-DEPTH AND PRESSURE-TIME PLOTS

The pressure-depth and pressure-time plots presented in Figures 3 and 4 were constructed for Oceanus with the following methodology. A seismic profile was extracted from the 3D seismic volume as an arbitrary line directed along the pipe trail. Key marker horizons on this profile were obtained from the results of previous studies (Cartwright et al. 2018; Kirkham et al. 2019) and were depth converted using interval velocities of 2000 m/s, 4,200 m/s, and 3000 m/s for the post-salt overburden (Pliocene to Recent), the salt layer (Messinian), and the pre-salt succession (Oligo-Miocene), respectively (Fig. 1B). These velocities were derived from data from nearby exploration wells (Kirkham et al. 2019).

Calculations of the hydrostatic and lithostatic pressure distribution with depth were based on a seawater density value of 1.06 g/cc, and 2.0, 2.15 and 2.35 g/cc for the post-salt, salt and pre-salt layers. The sediment densities were obtained from petrophysical measurements made on nearby wells in the Tamar Field (see Fig. 1A for location)(Needham et al. 2017). The fracture gradient for

the Oligo-Miocene sealing interval was taken from modelled values for the Tamar Field (Needham et al. 2017, their Fig. 19). This is the nearest borehole calibration of the Oligo-Miocene succession in the North Levant Basin. Although the fracture gradient is not an actual value, we note that it exceeds the mudweights used in the wells, and is based on actual drilling experience in multiple exploration and appraisal wells. The fracture gradient for the salt layer is taken as 2MPa below the lithostatic value. No actual measurements were available for the salt in the North Levant Basin (e.g. from leak-off tests or mini-fracture tests- see Needham et al. 2017). However, compilations of these test data from drilling across a variety of thick salt layers shows that the fracture gradient is close to the lithostatic gradient, or in some cases exceeds that value (Zhang and Yin, 2017). Our assumption of a fracture gradient set at 2 MPa below lithostatic is thus conservative, and accords with estimates of the upper limit of differential stress within salt layers of 1-3 MPa (Weijermaars and Jackson, 2014; Schoenherr et al., 2007).

The depth converted section along the Oceanus pipe trail was restored to its geometry at 1.7Ma (the time of formation of the first pipe in the trail) by removing sediments younger than this age from the post-salt overburden, but maintaining a constant water depth. The actual water depth is not known, but by keeping water depth constant, this simply requires a small amount of subsidence during the past 1.7Ma, which is consistent with stratigraphic analysis of depositional environments in this period (Gardosh and Druckman, 2006) and regional geological modelling (Al Balushi et al. 2016). In addition to this backstripping of post 1.7Ma sediments, the section was restored by retro-deforming Oceanus anticline such that the structural relief at the base salt diminished to zero. This equates to removing the mid-Pliocene to Recent phase of fold amplification (Kirkham et al. 2019) but does not involve any movement of the top salt surface, which remains horizontal throughout. Hence the restored profile (Fig. S3A) shows a thicker salt succession above the underlying

anticlinal axis than the present day section. The pressure-depth plot for this restored section (Fig. 3B) was constructed using the same input density values for the pre-salt, salt and post-salt layers as for the present day section. The fracture gradient within the Oligo-Miocene was adjusted to maintain a similar value (as a percentage of the lithostatic gradient) as in the pressure depth plot constructed based on the present day structural configuration (Fig. 3A).

The trap capacity of the Oceanus Structure at the present day was calculated (660m) by measuring the relief in metres from the spill point of the structure to the crest of the anticline as mapped at the reservoir level (Fig. S2). The trap capacity existing prior to the latest phase of fold amplification (340m) was obtained by subtracting the amplitude of the later phase of growth (equivalent to the structural relief at the base salt, 320m) from the present day trap capacity). Using these figures, indicative gas gradients were added to the two pressure-depth plots to show the minimal impact that a filled-to-spill gas column would have exerted on the top seal in comparison to the much larger aquifer overpressure (Fig. 3). The gas gradients were computed from measured gas pressures in appraisal wells on the Tamar Gas Field, where the reservoir is at a similar depth, and most likely similar pressure-temperature conditions as Oceanus (Needham et al. 2017).

The pressure-time plot was constructed by taking the two pressure-depth plots, and noting the intersection value of the fracture gradient with the depths to the top reservoir, and base salt for each plot. The critical pressure value was taken as the value at the top reservoir. These yielded 85.3 and 81.2 MPa, for the first and last pipe to form, respectively. Error bars on these values are estimated at ± 3 MPa, but would be systematic for both time steps since they are based on error bars for seismic correlation and depth conversion.

The pressure evolution in the last 1.7Ma was constructed by taking the dates of the individual fluids escape pipes (see below), and interpolating two contrasting sawtooth patterns (see main

text)(Kanno and Ichihara, 2018) between the starting and end point. In the first (Fig. 4B), the geometry of the ‘teeth’ is controlled by choosing a fixed pressure re-charge rate that matches rate during the build-up in overpressure leading to the first pipe forming event. The second (Fig. 4C) is defined by considering that the pressure drop for each ‘tooth’ is fixed and is equivalent to the fracture closure pressure or effective tensile strength (Hubbert, 1953). The effective tensile strength of the probable sealing claystones of the Oligo-Miocene are not known, but we set this to be 2 MPa, simply to illustrate one of many possible pressure evolutionary paths linking the two computed values.

SALT FLOW KINEMATICS

For Oceanus, the average flow velocity for the upper boundary of the salt layer was calculated from the biostratigraphic date for the horizon incised by the earliest pockmark, and the horizontal distance between the earliest and latest pockmark craters (3.4 km). These values give an average flow velocity of 2 (+/- 0.3) mm/a over the past 1.7 myrs (Cartwright et al. 2018). Pipe spacing was divided by average velocity for each individual trail to yield the timings of each pipe within each trail. These values were used to construct the pressure-time plot for Oceanus shown in Figure 4.

SUPPLEMENTARY FIGURES AND CAPTIONS

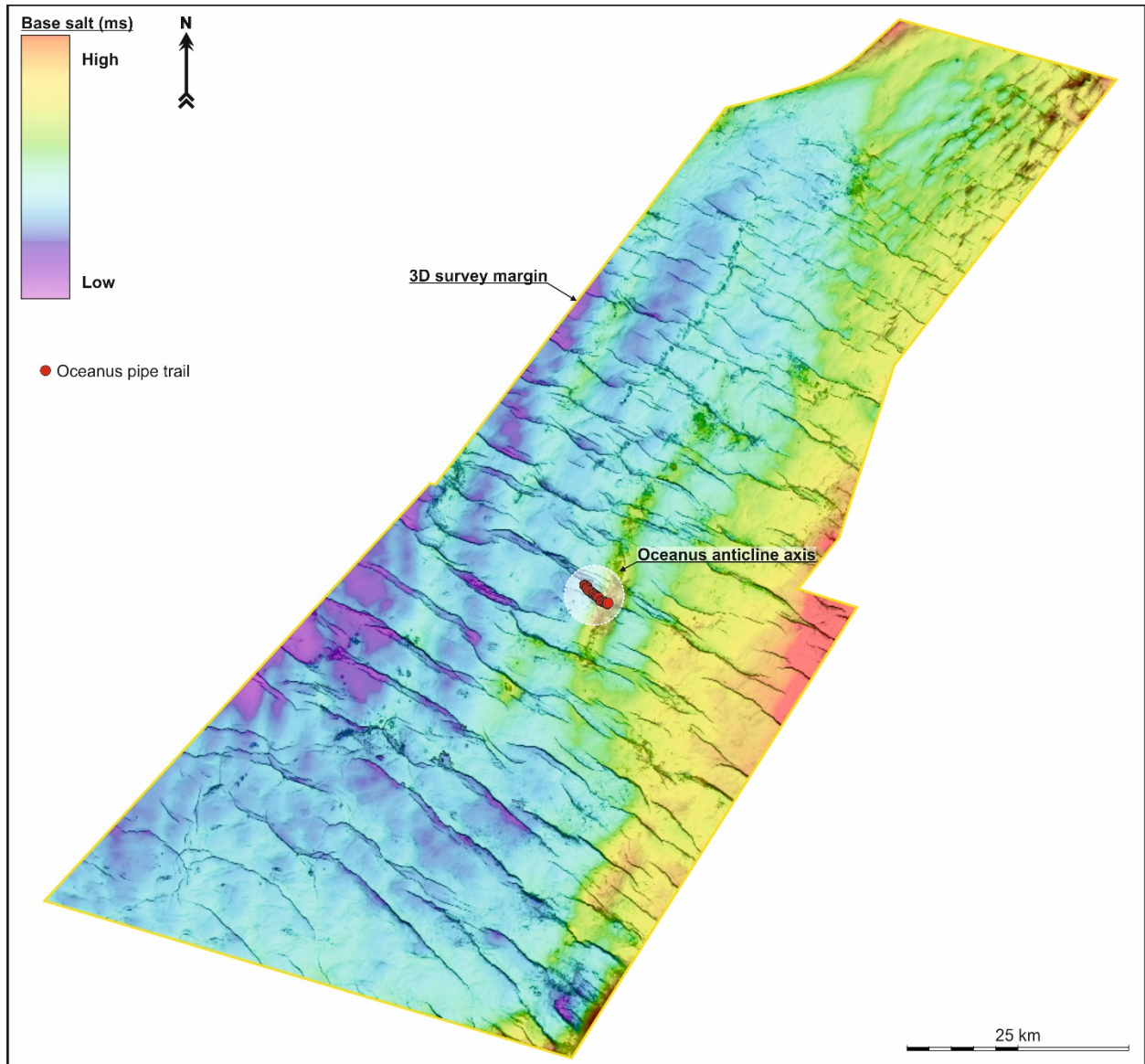


Figure S1: Two-way time Base Salt structure map (in milliseconds, ms) of the 3D survey in the study area, showing the location of the pre-salt anticline named Oceanus and the 21 fluid escape pipes that overly it. Also prominently visible are the WNW-ESE trending normal faults that are widely developed in the North Levant Basin.

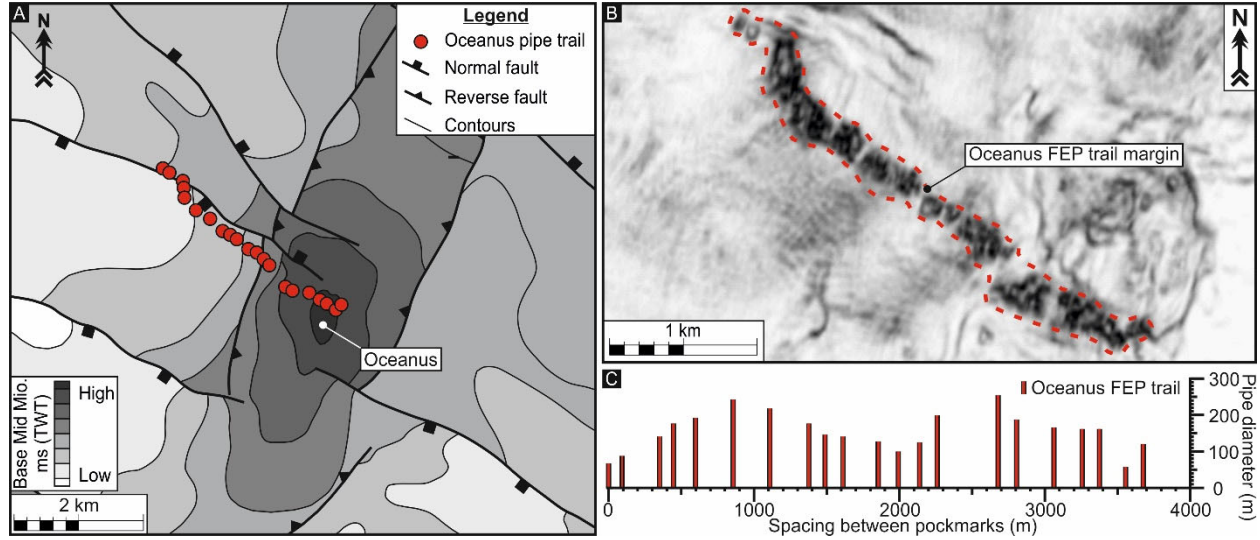


Figure S2: Detailed positions and spacing of the pockmarks associated with the fluid escape pipes trail overlying Oceanus. A: Structure map in two-way time (ms) of the Base Middle Miocene horizon (Modified from Cartwright et al. 2018) centred on Oceanus, showing the WNW orientation of the fluid escape pipe trail emanating from the crest of the anticline. The structure is aligned NNE-SSW, and bounded by reverse faults, and compartmentalised by WNW trending normal faults. B: A variance slice through the Pliocene to Recent overlying Oceanus, showing the WNW-ESE linear area of discontinuity attributed to the fluid escape pipe trail. C: Pockmark spacing data for the fluid escape pipe trail overlying Oceanus documented by Kirkham et al. (2019). These data were used to compute the ages of each pipe, for reconstruction of the pressure evolution over the past 1.7Myrs.

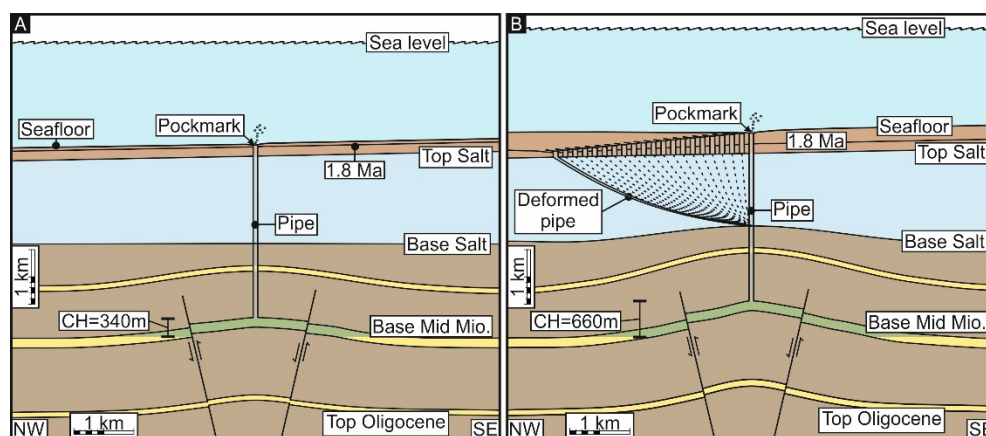


Fig. S3. Schematics of Oceanus and the fluid escape pipes at the first expulsion episode and most recent expulsion episode. A: A schematic restored depth cross-section of Oceanus at the timing (1.7 Ma) of initial pipe formation, with a trap capacity (CH=Column Height) of 340m. B: A schematic present day depth cross-section through Oceanus. Since initial pipe formation the top seal has episodically failed a further 20 time. Growth of the fold during the Pliocene to Recent has produced an increase in trap capacity to 660m, substantial structural relief at Base Salt and thinning of the overlying salt succession.

REFERENCES

- Al-Balushi, A. N., Neumaier, M., Fraser, A. J., and Jackson, C. A., 2016, The impact of the Messinian salinity crisis on the petroleum system of the Eastern Mediterranean: a critical assessment using 2D petroleum system modelling: *Petroleum Geoscience*, v. 22, p. 357-379, doi:10.1144/petgeo2016-054.
- Cartwright, J., Kirkham, C., Bertoni, C., Hodgson, N., and Rodriguez, K., 2018, Direct calibration of salt sheet kinematics during gravity-driven deformation: *Geology*, v. 46, p. 623-626, doi:10.1130/G40219.1.
- Cartwright, J., and Santamarina, C., 2015, Seismic characteristics of fluid escape pipes in sedimentary basins: implications for pipe genesis: *Marine and Petroleum Geology*, v. 65, p. 126-140, doi:10.1016/j.marpetgeo.2015.03.023.

Gardosh, M. A., and Druckman, Y., 2006, Seismic stratigraphy, structure and tectonic evolution of the Levantine Basin, offshore Israel: Geological Society, London, Special Publications, v. 260, p. 201-227, doi:10.1144/GSL.SP.2006.260.01.09.

Ghalayini, R., Nader, F., Bou Daher, S., Hawie, N., and Chbat, W., 2018, Petroleum systems of Lebanon: an update and review: Journal of Petroleum Geology, v. 41, p. 189-214, doi:10.1111/jpg.12700.

Gomez, F., Nemer, T., Tabet, C., Khawlie, M., Meghraoui, M., and Barazangi, M., 2007, Strain partitioning of active transpression within the Lebanese restraining bend of the Dead Sea Fault (Lebanon and SW Syria): Geological Society, London, Special Publications, v. 290, p. 285-303, doi:10.1144/290.10.

Hall, J., Calon, T., Aksu, A., and Meade, S., 2005, Structural evolution of the Latakia Ridge and Cyprus Basin at the front of the Cyprus Arc, eastern Mediterranean Sea: Marine Geology, v. 221, p. 261-297, doi:10.1016/j.margeo.2005.03.007.

Hubbert, M. K., and Willis, D. G., 1972, Mechanics of hydraulic fracturing: AIME Petroleum Transactions, Society of Petroleum Engineers, v. 210, p. 153-168.

Kanno, Y., and Ichihara, M., 2018, Sawtooth wave-like pressure changes in a syrup eruption experiment: implications for periodic and nonperiodic volcanic oscillations: Bulletin of Volcanology, v. 80, p. 65, doi:10.1007/s00445-018-1227-z.

Kirkham, C., Cartwright, J., Bertoni, C., Rodriguez, K., and Hodgson, N., 2019, 3D kinematics of a thick salt layer during gravity-driven deformation: Marine and Petroleum Geology, v. 110, p. 434-449, doi:10.1016/j.marpetgeo.2019.07.036.

Kirkham, C., Cartwright, J., Hermanrud, C., and Jebson, C., 2018, The genesis of mud volcano conduits through thick evaporite sequences: Basin Research, v. 30(2), p. 217-236, doi:10.1111/bre.12250.

Needham, D. L., Pettingill, H. S., and Christensen, C. J., 2017, The Tamar Giant Gas Field: Opening the Subsalt Miocene Gas Play in the Levant Basin: AAPG Special Volumes, v. 113, p. 221-256, doi:10.1306/13572009M1133688.

Schoenherr, J., Urai, J. L., Kukla, P. A., Littke, R., Schleder, Z., Larroque, J.-M., Newall, M. J., Al-Abry, N., Al-Siyabi, H. A., and Rawahi, Z., 2007, Limits to the sealing capacity of rock salt: A case study of the infra-Cambrian Ara Salt from the South Oman salt basin: AAPG bulletin, v. 91, p. 1541-1557, doi:10.1306/06200706122.

Weijermars, R., and Jackson, M. P., 2014, Predicting the depth of viscous stress peaks in moving salt sheets: Conceptual framework and implications for drilling: AAPG bulletin, v. 98, p. 911-945, doi:10.1306/09121313044.

Zhang, J., and Yin, S. X., 2017, Fracture gradient prediction: an overview and an improved method: Petroleum Science, v. 14, p. 720-730, doi:0.1007/s12182-017-0182-1.